ROYAL AEROSPACE ESTABLISHMENT

IMPROVEMENTS IN THE FORMULATION AND NUMERICAL SOLUTION OF THE EULER PROBLEM FOR SWEPT WINGS

by

M. F. Paisley

M. G. Hall

August 1988

Procurement Executive, Ministry of Defence
Farnborough, Hants

UNLIMITED

ROYAL AEROSPACE ESTABLISHMENT

Technical Memorandum Aero 2139

Received for printing 17 August 1988

IMPROVEMENTS IN THE FORMULATION AND NUMERICAL SOLUTION OF THE EULER PROBLEM FOR SWEPT WINGS*

by

M. F. Paisley

M. G. Hall

SUMMARY

A multigrid cell-vertex finite volume Euler method has been used to calculate steady inviscid transonic flow past the ONERA M6 wing. The treatment of the far-field boundary conditions includes the effect of velocity perturbations generated from Klunker's analytic asymptotic solution to the transonic small-disturbance equation. The geometry of the wing tip is modelled with three successively finer C-0 grids. The results obtained show marked differences in comparison with those obtained on C-H grids. They indicate that a shock-wave mechanism can contribute to the generation of tip vortices in compressible inviscid flow, and that for reliable prediction of wing performance it is important to model well both the wing-tip geometry and the flow around the tip.

---

* This paper was presented at IUTAM Symposium Transsonicum III, Göttingen, 24-27 May 1988.

LIST OF CONTENTS

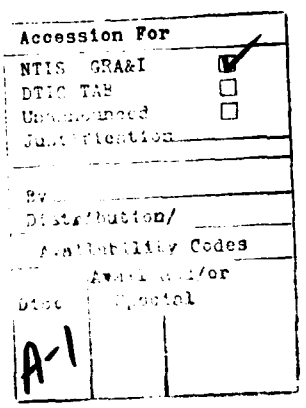

1 INTRODUCTION

The work of Ni[1] has been extended in two and three dimensions by Hall[2] and Salmond[3]. Numerical solutions to the Euler equations for transonic lifting flows past aerofoils and wings are obtained by approximating the steady flux balance for each computational cell using values of the flow variables stored at the vertices of each cell. A Lax-Wendroff time-stepping algorithm is used to update each variable, with boundary conditions where appropriate, and these changes in the solution are then used on coarser meshes to accelerate the convergence of the solution to the steady state. This paper describes some recent developments, mainly in the imposition of far-field boundary conditions and in the modelling of the flow around the wing tip.

The usual practice in calculating the three-dimensional flow past a wing has been to set conditions on the far-field boundary equal to the free-stream conditions. This assumption is loosely justified by the knowledge that, except in a wake, a disturbance would decay more rapidly with distance in three dimensions than in two. Here, instead, we replace the free-stream conditions by a three-dimensional far-field solution. For 'inflow' the conditions are derived from the transonic small-disturbance approximation of Klunker[4], while for 'outflow' a perturbation pressure related to the cross-flow in the numerical solution is prescribed. The results are expected to be more accurate than those given by assuming free-stream conditions and to provide an indication of the range of validity of the latter assumption. Comparisons are shown for a range of distances from the wing to the far-field boundary.

It is becoming recognised (for example, see Ref 5) that the resolution of flow detail at the wing tip requires both the representation of the tip geometry and the use of an appropriate grid around the tip. We outline here the steps taken in generating C-O grids from C-H grids formed by spanwise stacking of two-dimensional planar C-grids. Results are shown for calculations performed on the ONERA M6 wing using both C-H grids and three successively finer C-O grids. We begin however with an outline of the basic numerical method.

2 CELL VERTEX FINITE VOLUME EULER METHOD

Since only the steady state is of interest the unsteady Euler equations in three dimensions are expressed in conservation form as the isenthalpic system

$$\underline{u}_t + f(\underline{u})_x + g(\underline{u})_y + h(\underline{u})_z = 0 \quad , \tag{1}$$

where the state vector $\underline{u}$ and the flux vectors $\underline{f}(u)$, $\underline{g}(u)$, $\underline{h}(u)$ are given as follows:

$$\underline{u} = \begin{pmatrix} \rho \\ \rho u \\ \rho v \\ \rho w \end{pmatrix}, \quad f(\underline{u}) = \begin{pmatrix} \rho u \\ p + \rho u^2 \\ \rho uv \\ \rho uw \end{pmatrix}, \quad g(\underline{u}) = \begin{pmatrix} \rho v \\ \rho vu \\ p + \rho v^2 \\ \rho vw \end{pmatrix}, \quad h(\underline{u}) = \begin{pmatrix} \rho w \\ \rho wu \\ \rho wv \\ p + \rho w^2 \end{pmatrix}.$$

Here ρ is the density, u, v, w are Cartesian components of velocity and p is the pressure given by Bernoulli's equation

$$p = \frac{\rho}{\gamma}\left(1 - \tfrac{1}{2}(\gamma - 1)(u^2 + v^2 + w^2)\right) ,$$

where γ is the ratio of specific heats, taken to be 1.4. The equations have been non-dimensionalised with respect to a typical length, stagnation sound speed and stagnation pressure.

Integrating equation (1) over a control element of volume V and using the divergence theorem yields for the steady state the boundary integral (or residual)

$$\frac{1}{V}\iint (f,g,h).\underline{ds} = 0 . \qquad (2)$$

Dividing our region of physical space surrounding the wing into hexahedral cells we seek to approximate equation (2) for each cell. The fluxes through each of the faces of a particular cell are calculated from the values of the flow variables stored at the vertices of that cell (see Fig 1) and are summed to give the net flux into the cell.

Given an initial flow the steady solution $\underline{u}$ satisfying equation (2) for all cells is obtained by a Lax-Wendroff time-marching algorithm. From equation (1) the change in the solution, $\delta\underline{u}^n = \underline{u}^{n+1} - \underline{u}^n$, in time-step Δt is given by

$$\delta\underline{u} = -\Delta t(f_x + g_y + h_z) - \frac{\Delta t^2}{2}\left\{\frac{\partial}{\partial x}\left(\frac{\partial f}{\partial \underline{u}}\frac{\partial \underline{u}}{\partial t}\right) + \frac{\partial}{\partial y}\left(\frac{\partial g}{\partial \underline{u}}\frac{\partial \underline{u}}{\partial t}\right) + \frac{\partial}{\partial z}\left(\frac{\partial h}{\partial \underline{u}}\frac{\partial \underline{u}}{\partial t}\right)\right\} . \qquad (3)$$

The two parts of the change $\delta\underline{u}$ at the point P are calculated as follows (see Fig 2). The first term in expression (3) is given by averaging the residuals (2) for the eight cells surrounding P . The second term is recast by integrating over the inner hexahedron surrounding P formed by the centres of the eight cells. The divergence theorem again yields an integral over the surface of this hexahedron, evaluated as before, the values of the flow variables used being obtained as averages of the values at the vertices of the eight cells.

To prevent odd-even point decoupling and to capture shock-waves an artificial viscosity is added to $\delta\underline{u}$. Convergence acceleration is achieved using local time-stepping and a multigrid procedure. Changes in the solution on the coarse grids are interpolated linearly to the finer grids as previously but are then smoothed by an averaging operator.

3 FAR-FIELD BOUNDARY CONDITIONS

In the present method the inflow condition is that the two components of velocity in the plane locally tangential to the boundary are specified together with an isentropy condition for the density. To determine corrections to the free-stream condition in the far-field we firstly consider Klunker's expression for the transonic small-disturbance potential ϕ at a point $P(x,y,z)$. In the far-field Klunker shows that the dominant term is that representing the lifting effects of the wing, namely the following integral over the wing surface (see Fig 3)

$$\phi_p = \frac{z}{4\pi} \int_{\substack{\text{wing} \\ \text{surface}}} \frac{\Delta u}{(y-\eta)^2 + z^2} \left(1 + \frac{x-\xi}{R}\right) dS \quad , \tag{4}$$

where ξ, η are local coordinates on the wing and $R^2 = (x-\xi)^2 + \beta^2(y-\eta)^2 + \beta^2 z^2$ with $\beta^2 = 1 - M_\infty^2$. Δu is interpreted here as the difference in pressure between the upper and lower surfaces. Due to deficiencies in the potential model ϕ_p is only a good approximation away from the wake, and in fact is only used to generate perturbations to the velocities given at 'inflow'.

ϕ_p is differentiated to give expressions for the perturbations $(\delta u, \delta v, \delta w)$ from the free-stream velocities $(u_\infty, v_\infty, w_\infty)$. The resulting integrals are evaluated numerically for each point P on the 'inflow' part of the far-field boundary. The modified velocities $(u_\infty + \delta u,\ v_\infty + \delta v,\ w_\infty + \delta w)$ are then used to calculate the two imposed components of the tangential velocity. If the perturbations are set to zero we regain the free-stream boundary conditions.

At outflow a boundary condition on pressure p is assumed which includes the effect of the component of velocity q_n normal to the free-stream direction. It can be shown that if variations in the function p/ρ^γ are small, and if at outflow

$$u^2 + v^2 + w^2 = q_\infty^2 + q_n^2 \quad ,$$

where q_∞ is the free-stream velocity, then the Bernoulli equation can be approximated by

$$p = \left(p_\infty^{(\gamma-1)/\gamma} - \frac{\gamma - 1}{2} q_n^2 \right)^{\gamma/(\gamma-1)} \quad .$$

This is the assumed condition.

4 WING TIP MODELLING

The stages in producing a C-O grid from the C-H grid comprising two-dimensional planar C-grids stacked spanwise are as follows:

(i) discard the C-grids lying beyond the wing tip;

(ii) complete the surface closure for the M6 wing using circular arcs as continuations of the wing generators. The (finest) surface grid has each arc subdivided into 32 equal segments;

(iii) as sketched in Fig 4, rotate the C-grid corresponding to the tip station 180° about an axis running chordwise through the leading and trailing edges. Equal subdivision of the arcs swept out provide the field grid. Lines of semi-polar singularity are left along the axis of rotation forward of the leading edge and aft of the trailing edge.

After these steps adjustments were made to produce the final grid. These included bending and packing of the C-grids to ensure smooth spanwise distributions, the addition of a further 16 C-grids on the main wing, and contracting the grid around the trailing edge of the tip where the tip radius is small. Thus from an original C-H grid of 256 × 32 × 48 cells was produced a new C-O grid of 256 × 32 × 64 cells. Details of the medium grid (128 × 16 × 32) on the wing surface near the tip are shown in Figs 5 and 6.

5 RESULTS

The numerical method was used in two forms, appropriate to the C-H and C-O grids, to calculate the flow past the ONERA M6 wing, with $M_\infty = 0.84$ and

$\alpha = 3.06^{\circ}$. To evaluate the effect of the new boundary conditions the far-field boundary was set at varying distances from the wing - 1.01, 1.69 and 3.37 spans (3, 5 and 10 root chords respectively) - and the calculations performed with and without the perturbations modifying the free-stream. The effect on C_L is shown in Fig 7 for the calculations on the medium C-H and C-O grids. With the free-stream conditions the variation in C_L is around 3% while for the perturbed conditions it is around 0.7%. All subsequent calculations were performed with the perturbed conditions with the boundaries set at 1.69 spans.

Next we detail the comparison between the tip flows on the medium C-H and C-O grids. The spanwise lift distributions in Fig 8 show a marked spike at the tip for the calculation on the C-H grid, indicating a vortex. This is absent for the calculation on the C-O grid and examination of the cross-flow shows little sign of a vortex, although the cross-flows are much larger than for the C-H grid. Shown in Figs 9 and 10 are the upper surface Mach number contours in the tip region for the two cases. As might be expected the flows are very similar inboard but quite different at the tip. For the calculation on the C-O grid the contours near the tip trailing edge indicate the presence of high velocities there.

Finally we compare the calculations performed on the successively finer C-O grids. Fig 11 shows the value of C_L plotted against (number of cells)$^{-2/3}$, the straight line indicating second-order accuracy. The spanwise lift distributions are plotted in Fig 12. Note the small kink at the tip for the finest grid; indeed (Fig 13) a plot of the cross-flow velocities obtained on this grid, very close to the trailing edge (98.5% chord), shows a region of recirculating flow.

The production of the recirculating flow, or tip vortex, can be explained by examining the cross-flow upstream. Having become sonic at about 89% chord the cross-flow Mach number reaches 3.0 at 96.5% chord. A shock in the cross-flow plane can be seen in the velocity vectors and in the contours of cross-flow Mach number in Figs 14 and 15 obtained on the finest grid. The corresponding plot of total vorticity contours in Fig 16 shows that while some vorticity is produced at the junction of the circular arc with the wing generator, more is produced through the shock-wave. This vorticity is convected downstream and may therefore be the origin of the vortex shown. Further work needs to be done to assess whether separation is occurring in addition.

The marked differences between the results on the C-O grid and those on the C-H grid have important practical implications. They show that the flow pattern around the wing tip and the associated spanwise lift distribution are strongly

misrepresented when calculations are performed on the commonly adopted C-H grid. For reliable prediction of wing performance the wing-tip geometry and the flow around the tip must be well modelled, at least for wings of low aspect ratio.

6 CONCLUSIONS

Improved far-field boundary conditions and wing tip modelling have been proposed and tested. The boundary conditions allow the distance to the far-field boundary to be reduced considerably with little change in lift. Calculations on C-H and C-O grids show very marked differences in the flow at the wing tip, there being a distinct tip vortex on the C-H grids. Although cross-flows are much larger on the C-O grids there is little sign of a tip vortex except for the finest grid. In this case a vortex appears to originate at least in part in vorticity generated by a shock in the cross-flow. For reliable prediction of wing performance it is important to model well both the wing-tip geometry and the flow around the tip.

Acknowledgments

The authors thank Cray Research (UK) Ltd and AERE Harwell for providing assistance and computing facilities essential for the completion of the work described.

REFERENCES

No.	Author	Title, etc
1	R.-H. Ni	A multiple grid scheme for solving the Euler equations. *AIAA J.*, 20, 11, 1565-1571 (1982)
2	M.G. Hall	Cell-vertex schemes for solution of the Euler equations. Proc. Conf. on Num Meth for Fl Dyn, University of Reading, 1985, (Eds. K.W. Morton and M.J. Baines) Oxford University Press, 303-345 (1986)
3	D.J. Salmond	A cell-vertex multigrid scheme for solution of the Euler equations for transonic flow past a wing. Proc. ICNMFD 10, Beijing, China, 1986 (Eds. F.G. Zhuang and Y.L. Zhu) Springer-Verlag Lecture Notes in Physics No.264, 549-553 (1986)
4	E.B. Klunker	Contribution to methods for calculating the flow about thin lifting wings at transonic speeds - analytic expressions for the far-field. NASA TN D-6530 (1971)
5	P. Sacher	Numerical solutions for three-dimensional cases - swept wings. Chapter 7, "Test cases for inviscid flow field methods". AGARD Advisory Report No.211 (1985)

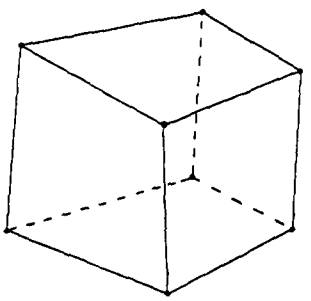

Fig 1 A single hexahedral cell

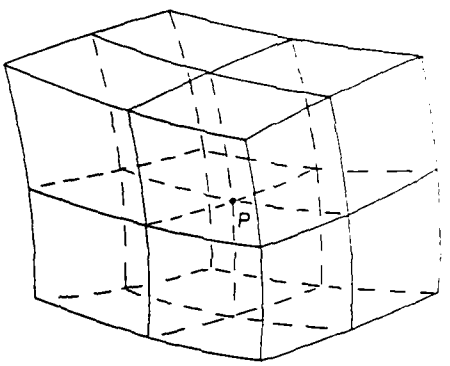

Fig 2 The eight cells surrounding the point P

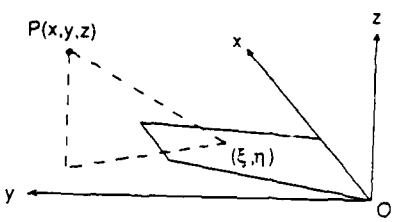

Fig 3 Wing and a boundary point P for Klunker's integral over the wing surface

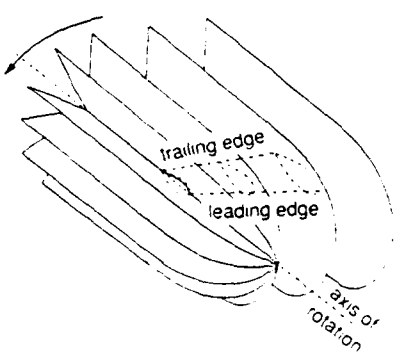

Fig 4 Sketch of construction of C-O grid from C-H grid by rotation

Figs 5-10

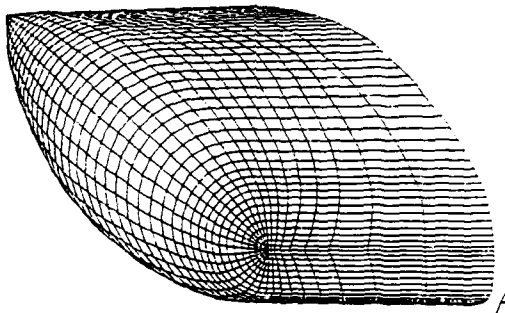

Fig 5 Surface grid at the wing tip (leading edge)

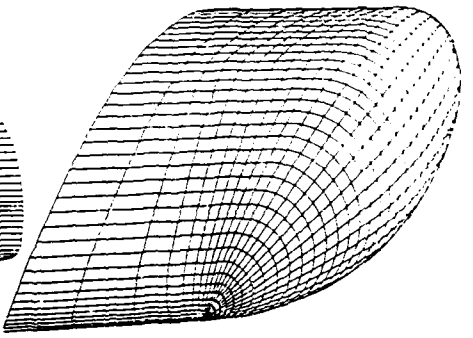

Fig 6 Surface grid at the wing tip (trailing edge)

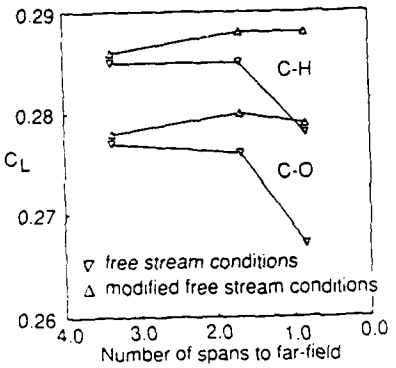

Fig 7 Variation of lift with position of far-field boundary

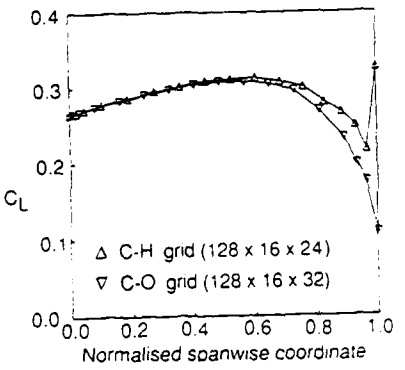

Fig 8 Spanwise lift distributions for calculations on the medium C-H and C-O grids

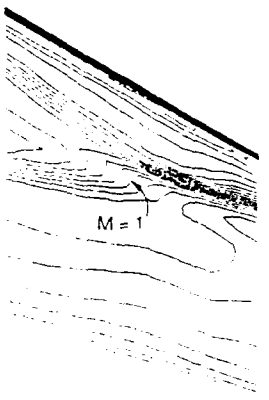

Fig 9 Mach contours on upper surface for the calculation on the medium C-H grid (Δ M = 0.04)

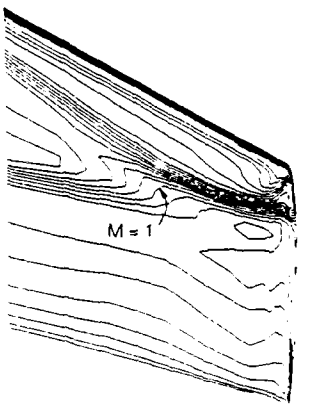

Fig 10 Mach contours on upper surface for the calculation on the medium C-O grid (Δ M = 0.04)

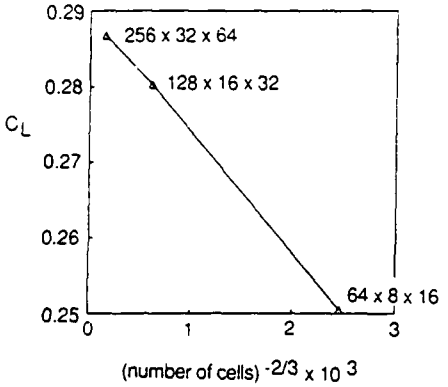

Fig 11 Variation of C_L with refinement of the C-O grid

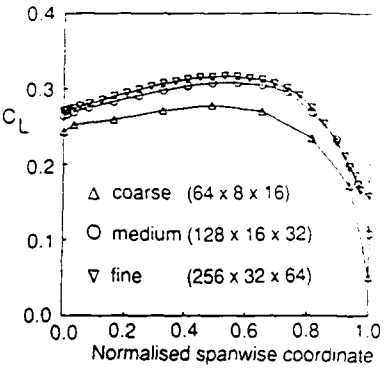

Fig 12 Variation of the spanwise lift distribution with refinement of the C-O grid

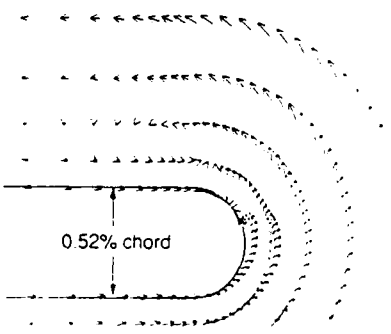

Fig 13 Cross-flow velocity vectors at the wing tip very near the trailing edge (98.5% chord)

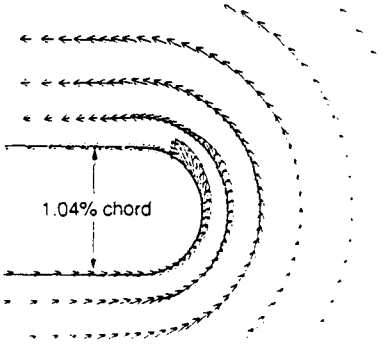

Fig 14 Cross-flow velocity vectors at the wing tip near the trailing edge (96.5% chord)

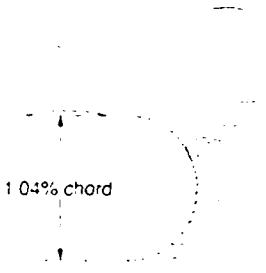

Fig 15 Cross-flow Mach contours at the wing tip near the trailing edge (96.5% chord)
Dotted line is sonic and $\Delta M = 0.2$

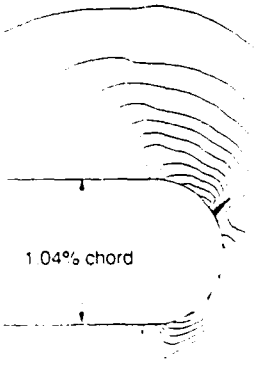

Fig 16 Vorticity ($|\Omega|$) contours at the wing tip near the trailing edge (96.5% chord)

REPORT DOCUMENTATION PAGE

Overall security classification of page

UNLIMITED

As far as possible this page should contain only unclassified information. If it is necessary to enter classified information, the box above must be marked to indicate the classification, e.g. Restricted, Confidential or Secret.

1. DRIC Reference (to be added by DRIC)	2. Originator's Reference	3. Agency Reference	4. Report Security Classification/Marking
	RAE TM Aero 2139		UNLIMITED

5. DRIC Code for Originator	6. Originator (Corporate Author) Name and Location
7673000W	Royal Aerospace Establishment, Farnborough, Hants, UK
5a. Sponsoring Agency's Code	6a. Sponsoring Agency (Contract Authority) Name and Location

7. Title: Improvements in the formulation and numerical solution of the Euler problem for swept wings

7a. (For Translations) Title in Foreign Language

7b. (For Conference Papers) Title, Place and Date of Conference

IUTAM Symposium Transsonicum III 24-27 May 1988, Göttingen, W. Germany.

8. Author 1. Surname, Initials	9a. Author 2	9b. Authors 3, 4 ...	10. Date	Pages	Refs
Paisley, M.F.	Hall, M.G.		August 1988	12	5

11. Contract Number	12. Period	13. Project	14. Other Reference Nos.

15. Distribution statement

(a) Controlled by

(b) Special limitations (if any)

If it is intended that a copy of this document shall be released overseas refer to RAE Leaflet No.3 to Supplement 6 of MOD Manual 4.

16. Descriptors (Keywords) (Descriptors marked * are selected from TEST)

Finite volume; Swept wing; Far-field boundary conditions; Wing tip modelling; Vortex generation; Euler equations; Transonic flow; Boundary value problems. Shock waves (cds)

17. Abstract

A multigrid cell-vertex finite volume Euler method has been used to calculate steady inviscid transonic flow past the ONERA M6 wing. The treatment of the far-field boundary conditions includes the effect of velocity perturbations generated from Klunker's analytic asymptotic solution to the transonic small-disturbance equation. The geometry of the wing tip is modelled with three successively finer C-O grids. The results obtained show marked differences in comparison with those obtained on C-H grids. They indicate that a shock-wave mechanism can contribute to the generation of tip vortices in compressible inviscid flow, and that for reliable prediction of wing performance it is important to model well both the wing-tip geometry and the flow around the tip.